*Electronic Supplementary Information for*

# Chitosan Biopolymer-F(ab´)$_2$ Immunoconjugate Films for Enhanced Antigen Recognition

*João Borges,* José M. Campiña,* A. Fernando Silva*

Centro de Investigação em Química (CIQ-L4), Departamento de Química, Faculdade de Ciências,

Universidade do Porto, Rua do Campo Alegre 687, 4169-007 Porto, Portugal



**Corresponding author:* José Miguel Campiña, Email: jpina@fc.up.pt; João Borges, Email: jborges@fc.up.pt

# S1 Extended Description of Materials and Methods

## S1.1 Chemicals

3-mercaptopropionic acid (Sigma-Aldrich); affinity isolated F(ab´)$_2$ fragment of Anti-Human IgG produced in goat (specific to the Fab fragment of human IgG, Sigma-Aldrich); Purified human immunoglobulin G (HIgG, lyophilized powder, >95%, Sigma Aldrich) and all other chemicals were analytical grade and used as received. Chitosan ChitoClear$^{TM}$ TM2455 (extracted from coldwater shrimps and treated to a degree of deacetylation of DD=95%, molecular weight in the range 150-200 kDa; Chit95) was purchased to Primex (Siglufjordur, Iceland).

Other chemicals involved in the realization of this study involve: Sodium dihydrogen phosphate (Sigma-Aldrich, ≥ 99%,); Sodium hydrogen phosphate (Sigma-Aldrich, ≥ 99%,); Glacial acetic acid (Sigma Aldrich, >99%); Sodium acetate trihydrate (Merck suprapur); Sodium chloride (Sigma-Aldrich, >99.9%); Nitric acid (Pronalab, 69%,); Hydrochloric acid (Fluka, >37%); Ethanol (Aga, 96% vol.); Potassium hexacyanoferrate (II) tryhidrate (≥ 99.5%, Fluka); Potassium hexacyanoferrate (III) (> 99%, Merck);; $N_2$ (N45, Air Liquide); Hydrogen peroxide (30%, p.a., Fluka); Sulfuric acid ($H_2SO_4$, 95-97%, Fluka).

## S1.2 Stock Solution Concentrations

All the aqueous solutions were prepared with ultrapure water from a Millipore purification system (resistivity >18.2 MΩ·cm). F(ab´)$_2$ and HIgG stock solutions were prepared in phosphate buffer saline (PBS) 0.01 M (pH=6.85). Whereas F(ab´)$_2$ did not require reconstitution in the presence of salt in order to prepare a stock solution, incubation of HIgG in pure NaCl 150 mM solution and its further dilution with PBS (without NaCl) to the desired concentration, led to the formation of highly turbid solutions even after hours of stirring. The data was taken as strong evidence supporting the unfolding of the protein in simultaneous with the dilution of the salt.

Thus, an approximate 1 mg·mL$^{-1}$ HIgG solution was prepared in PBS 0.01 M + NaCl 150 mM to ensure the proper reconstitution and functionality of the protein. With all, some aggregates (corresponding to a small fraction of non-reconstituted

proteins) were still eye-witnessed in the solution. To sediment these aggregates, the solution was subsequently centrifuged at 16000g (25ºC) during 30 min using a Galaxy 16DH (VWR). The supernatant was, then, recovered and the concentration measured from UV-Vis measurements.

Spectroscopic measurements were performed at 280 nm in a Hitachi U-300 spectrophotometer. The protein's concentration in solution can be calculated from its absorbance by means of the Beer´s law:

$$C = A_{280}/L\varepsilon \qquad (1)$$

where $A_{280}$ is the solution absorbance, C is the protein concentration (given in $mg \cdot mL^{-1}$ always that ε is given as a percent extinction coefficient in $mg^{-1} \cdot mL \cdot cm^{-1}$; i.e. it can be taken as the absorbance at 280 nm of a 1 $mg \cdot mL^{-1}$ solution of the corresponding protein; $\varepsilon = A_{280nm}^{1mg/mL}$), and L is the path length of the quartz cuvettes (1 cm). A typical value reported for IgGs, was assumed for the calculations: $A_{280nm}^{1mg/mL} = 1.4$ [1]. Thereby, the concentration of $F(ab')_2$ and HIgG stock solutions were determined to be 129 and 874 $mg \cdot mL^{-1}$, respectively. In the latter case, it was adjusted to 500 $mg \cdot mL^{-1}$ by dilution with the proper amount of PBS 0.01 M + NaCl 150 mM solution.

### S1.3 Detailed Preparation of Chitosan-Decorated Au Plates and Electrodes

5 MHz overtone polished AT-cut plano-plano quartz crystals with a diameter of 14 mm coated with gold electrodes of 0.785 $cm^2$ on both sides were used in QCM-D experiments. Measurements were performed at a data collection rate of 1 $datapoint \cdot s^{-1}$ and 25.00 ± 0.01 ºC. Prior to each experiment the gold-covered quartz plates were cleaned at room temperature (20º C) with freshly prepared piranha solution (3:1 = $H_2SO_4$/30% $H_2O_2$, v/v) for 2 min to remove impurities, later rinsed with large amounts of ethanol and Millipore water, and then dryed under a stream of nitrogen. *Piranha solution is very corrosive, reacts violently with organic materials and utmost care should be taken and proper protective clothing should be used when handling it. Piranha solution should*

*be handled with extreme care, and only small volumes should be prepared at any time.* In all cases, the quartz crystals were used immediately after the cleaning process.

The methodology used to prepare the modified surfaces consists in the well-known Layer by Layer (LbL) deposition of oppositely charged polyelectrolytes. The QCM-D crystals were inserted into the cell exposing just one side of the quartz plate for measurements. After probe equilibration in air, and then in ethanol, a 1 mM MPA solution in ethanol was injected into the QCM-D cell and the variations in $f$ and $D$ were registered until stabilization. Proper equilibration was indicated by cessation of any significant further decrease in the frequency of the plates. Afterwards, pure acetate buffer 0.05 M (pH=5.5) was injected until equilibration. Then the deposition of Chitosan was performed by injection of a 1 mg·mL$^{-1}$ Chit95 solution in the same buffer into the cell. After MPA deposition, and previous to equilibration in the liquid phase (acetate buffer), the plates were removed from the cell and rinsed with ultrapure water and ethanol, and dried under $N_2$ for further ex-situ characterization. Good stability and reproducibility have been demonstrated for chitosan films prepared in this way [2]. For adsorption onto Au/MPA surfaces, F(ab´)$_2$ was injected (after equilibration in the corresponding buffer) in the following range of concentrations: $C_{Fab2}$=0.03-128.6 µg·mL$^{-1}$. A $C_{Fab2}$=15.2 µg·mL$^{-1}$ solution was injected for 10 h in order to prepare the Au/MPA/F(ab´)$_2$ and Au/MPA/Chit95/F(ab´)$_2$ used in piezoelectric interrogation. These studies consisted of the injection of HIgG solutions (prepared by dilution of stock solution with 0.01 M PBS + 150 mM NaCl buffer with the following concentrations: $C_{HIgG}$=0.02, 0.36, 10.15, 37.34, 53.85, 76.53, and 103.40 mg·mL$^{-1}$) into the QCM-D cell containing the F(ab´)$_2$-modified plates.

All the CV electrochemical experiments were registered within a the potential range of -0.3 and +0.6 V at a scan rate of 50 mV·s-1 and 25 ºC. A conventional three-electrode cell (equipped with an helix-shaped gold wire counter-electrode and a Ag/AgCl/KCl sat. reference electrode) was used in all CV and EIS experiments. A rod-shaped Au polycrystalline working electrode, previously cleaned by the application of consecutive cycles of annealing in a butane flame and subsequent potential cycling in 0.1 M $HClO_4$ until the typical profile of polycrystalline gold was obtained [3], was used in all cases. A surface area of 0.11 ± 0.05 cm$^2$ was previously estimated by the method of the

electrochemical reduction of an AuO monolayer [4,5]. The contact between the electrode surface and the solution was made by means of the hanging meniscus method [6]. The clean and ordered electrode was previously coated with a self-assembled monolayer of MPA by overnight immersion in a 1 mM solution of MPA in ethanol. Posterior modification with a layer of colloidal chitosan was also performed through the dip-coating procedure by immersing the Au/MPA electrode in the 1 mg·mL$^{-1}$ Chit95 solution in 0.050 M acetate buffer (pH 5.5) for 30 min. Adsorption of F(ab´)$_2$ onto either Au/MPA or Au/MPA/Chit95 electrodes was performed by 15 h incubation from a 15.2 μg·mL$^{-1}$ F(ab´)$_2$ solution in PBS. Electrochemical interrogation of the resulting surfaces was performed upon successive additions of HIgG stock solution covering a concentration range analogous to that investigated in the piezoelectric tests. After each HIgG injection, the F(ab´)$_2$-modified electrodes were incubated for 10 min before measurements.

# S2 Preparation and Characterization of Model Substrates

## S2.1 Frequency Changes and Energy Dissipation data

The shifts in resonance frequency ($Df_n$) were measured, in simultanous with the shifts in the dissipation factor ($DD_n$), during the deposition of the different layers composing the Au/MPA/Chit95 surfaces by means of the QCM-D technique (Figures S1, S2, S3, and S4).

## S2.2 Atomic Force Microscopy

Topographic 5 x 5 μm$^2$ AFM pictures recorded in tapping mode at the different stages of the modification of the Au-covered plates with the MPA and Chit95, are presented in Figure S5. The statistical information on the roughness, height, and particle size derived from them are shown in Table S1.

## S2.3 Contact Angle

The wettability of the Au substrates functionalized with MPA, and MPA/Chit95 was determined in air through the static sessile drop method using a contact angle goniometer formed by an Olympus SZH8 zoom microscope coupled to a Panasonic WV-BL200 camera. Optimas v4.01 software was run for data acquisition. Ultrapure water was used as the liquid phase. The analysis of surface-drop contact angles was done using the free

software Image J. Contact angle measurements were taken at room temperature for three ultrapure water drops (of 5 μL) and averaged for each surface. The standard deviation was taken as the corresponding errors (see Table 1 in the manuscript). The images obtained are presented in Figure S6.

## S3 The Sauerbrey´s equation

According to Sauerbrey et al. [7], the shift in the vibration frequency ($\Delta f$) suffered by a quartz plate in air is associated to both changes in the crystal and in the deposited mass ($\Delta m$) on it:

$$\Delta f_n / n = [-2 f_0^2 / A (p_q m_q)^{1/2}] \Delta m = -(C_f/A) \Delta m \quad (2)$$

which can be re-organized to:

$$\Delta m/A = -(1/C_f) \Delta f_n/n \quad ---> \quad r = -C \Delta f_n/n \quad (3)$$

where $f_0$ is the resonant frequency of the quartz plate (here 5 MHz), $A$ the piezoelectrically active area (defined by the gold covered surface, $A$ = 0.785 $cm^2$), $p_q m_q$ the product of the density (2.648 g $cm^{-3}$) and the shear modulus of quartz ($2.947 \times 10^{11}$ g $cm^{-1}$ $s^{-2}$) respectively, and $n$ the overtone number. $C_f$ is called the sensitivity factor of the crystals and has a value of 55.5 Hz $mg^{-1}$ $cm^2$ at room temperature for the quartz plates previously described, and $C$ is its reciproque $1/C_f$

Equation 2 supposes that the deposited mass must be rigid (with no energy dissipation) and evenly distributed. Thin films meeting these requirements ensure that viscoelastic effects and/or overadsorption do not affect significantly the results, thus, enabling the application of equation 3 for the quantitative analysis of the adsorption phenomena.

We found in previous research on the adsorption of β-Lactoglobulin (b-LG) that, under certain experimental conditions, large protein self-aggregates can be formed turning the films highly viscoelastic and unable to follow the oscillation rigidly [2]. This behavior agrees well with that observed in the adsorption of other proteins on solid surfaces [8-10]. Under these conditions the dissipation energy can change significantly and it must be taken into consideration to make a complete interpretation of the adsorption phenomena. As better discussed in the manuscript, limitations for

the quantification of mass changes, when working with proteins, arise from trapped water. This is an important factor leading to the overstimation of the mass measured by QCM and has to be handled with care.

## S4 Kinetics of Protein Adsorption: Random Sequential Adsorption Theory

Adsorption of $F(ab')_2$ onto Au/MPA surface was analyzed using a simplified form of the Random Sequential Adsorption (RSA) model. But let us evaluate in first place, the viability of using a much simpler formalism such as the Langmuir kinetic model. According to the latter, the adsorption rate, $d\theta\ dt^{-1}$, is reduced with decreasing the amount of available binding sites ($1\text{-}\theta$) on the surface. Supposing irreversible adsorption this kinetic law can be expressed as:

$$\frac{dq}{dt} = k_{ON} C_{Fab\,2} (1 - q) \tag{4}$$

It is implicitly assumed that the surface is composed of a finite number of adsorption sites and that each molecule can interact only with one of these sites (site-specific adsorption), otherwise the available area for the adsorption of a new particle cannot be longer given by $(1\text{-}\theta)$. Large molecules such as proteins occupy a large number of sites (non-site-specific) and the surface needs to be treated as a continuum ("planar" or "molecularly flat" surface). This is usually done using an empirical generalized Langmuir equation:

$$\frac{dq}{dt} = k_{ON} C_{Fab\,2} \left(1 - \frac{q}{q_{Max}}\right) \tag{5}$$

However, there is a general agreement in the field that this formalism is not adequate to describe protein adsorption phenomena. The Langmuir model can not account for certain kind of phenomena related with the non-site-specific nature of the adsorption process, such as surface exclusion effects induced by pre-adsorbed proteins (often referred to as negative cooperativity).

Substituting the term $[1\text{-}(\theta/\theta_{Max})]$ by a function $\Phi(\theta)$, so-called the available surface function, which provides with a more realistic depletion of surface sites and

consider the adsorption of protein to random surface sites may overtake some of the limitations of the Langmuir model. Up to date an exact solution for this function has been just obtained for the one dimensional (1D) adsorption problem, the so-called *Random Parking* [11]. Talbot and Schaaf derived an approximate solution for the 2D problem considering hard discs to model the particles [12]:

$$\Phi(q) = \frac{(1 - \frac{q}{q_j})^3}{[1 - ((0.812(\frac{q}{q_j}) + (0.2336(\frac{q}{q_j})^2) + (0.0845(\frac{q}{q_j})^3)]} \quad (6)$$

The results obtained with this function correlated well with simulations performed using Monte Carlo methods and experimental data obtained by Ramsden measuring the phase velocities of guided modes in optical waveguides upon which proteins were allowed to adsorb from solution [13]. The simulations yielded a saturation limit or jamming limit ($\theta_j$) at the 54.7 % which indicates the formation of a layer highly disordered. This is due to the fact that proteins can adsorb at any free position on the surface. As a consequence, adsorption on most of the remaining free positions may be hindered after exceeding a certain coverage due to steric repulsions between solution and adsorbed proteins. This phenomenology seems more realistic than the Langmuir model which restricts the adsorption to discrete binding sites.

Expresing the surface coverage in terms of the mass density won by the system upon the adsorption ($r$), equation 5 turns into:

$$\frac{dr}{dt} = k_{ON} C_{Fab\,2} (1 - \frac{r}{r_{Max}}) \quad (7)$$

where $k_{ON}$ is the rate constant for the adsorption process in cm·min$^{-1}$, $C_{Fab2}$ is the bulk concentration of F(ab´)$_2$ in ng cm$^{-3}$, and $\rho_{Max}$ the change in surface mass density in ng cm$^{-2}$ when the surface is completely filled and the time ($t$) is given in min.

Belfort et al have recently introduced a more simple form for the probability function, $\Phi(r)=(1+A@r)$ [14], in an study regarding the adsorption of proteins onto metallic surfaces. In this expression $A$ is a constant referred to as the steric factor, i.e.

a measure of the steric hindrance felt by proteins in their way to the surface. Thereby, one of the simplest forms of the so-called Random Sequential Adsorption (RSA) model can be reached by replacing *[1-(ρ/$p_{Max}$)]* by *(1+A·ρ)* in equation 7:

$$\frac{dr}{dt} = k_{ON} C_{Fab\,2}[1 + (Ar)] \tag{8}$$

Provided that the units discussed above for the rest of parameters are kept, *A* is given in $cm^2\ ng^{-1}$. Integration of this kinetic law leads to:

$$r = \frac{1}{A}(e^{2.3Ak_aC_bt} - 1) \tag{9}$$

Protein adsorption is often kinetically compared with polymer adsorption processes in the sense that a rearrangement step is required [15]. In line with this view, protein adsorption is thought to involve two steps: (a) fast initial attachment of proteins to the surface and (b) much slower structural rearrangements. Nowadays it is accepted that proteins can follow conformational or orientational changes, with or without augmentation of their footprints, upon contact with a surface owing to the establishment of favorable surface–protein interactions and the large entropic gain [16, 17]. As evidenced in Fig S8, two different regimes are established during the adsorption of $F(ab')_2$ (with exception of the two lowest concentrations studied in this work) which justifies the inclusion of a second step in the RSA model considered in equations 7-9. Two-step kinetic laws have been successful in the modeling of polymer adsorption data. Consequently, a double exponential equation seems more suitable for the kinetic fittings:

$$r = \frac{1}{A_1}(e^{2.3A1k_1C_{Fab\,2}t} - 1) + \frac{1}{A_2}(e^{2.3A2k_2C_{Fab\,2}t} - 1) \tag{10}$$

Each exponential in this equation aims to reflect the behavior observed at each of the kinetic regimes identified. Although the RSA model accounts for the typical delay due to surface exclusion effects [18], it can fail in the prediction of positive cooperative effects as those involved in the preferential adsorption of proteins in the neighborhood of other pre-adsorbed molecules. In this respect, Minton showed that a good balance between positive and negative cooperative effects can also lead to exponential Langmuir-type kinetic curves [19, 20]. It seems to be the case presented here. Thus, the exponential

character of equations 9 and 10 turns them into suitable expressions to fit the experimental data without the explicit consideration of positive cooperativism in the model (an advantage given the mathematical complexity of Minton's model). With all, equation 10 provided, by far, much better fitting to the experimental data obtained as deduced from the comparison between Fig S7 and Fig 1b in the manuscript.

## S5. Randles-type Equivalent Circuit

Considering an electrochemical system for which nor the electron transfer nor the semi-infinite diffusion are the rate determining step, the process is said to operate under mixed control. Such a kind of system can be modeled by incorporating a Warbourg impedance element to the Randles circuit. Such a derived circuit (see the schematic represation following this paragraph) consists of a resistance ($R_1$, accounting for the electrolyte resistance) in series with an element formed by a CPE (accounting for the topological imperfections of the rough electrode surfaces) in parallel with a second resistance ($R_2$, the apparent charge transfer resistance across the interface) and a Warburg diffusion impedance element ($W$)

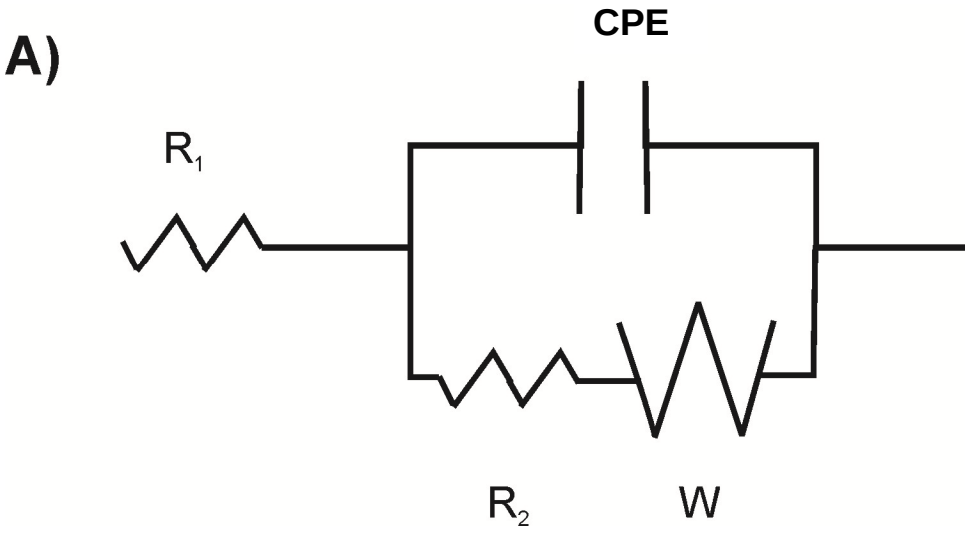

# S6. Figures

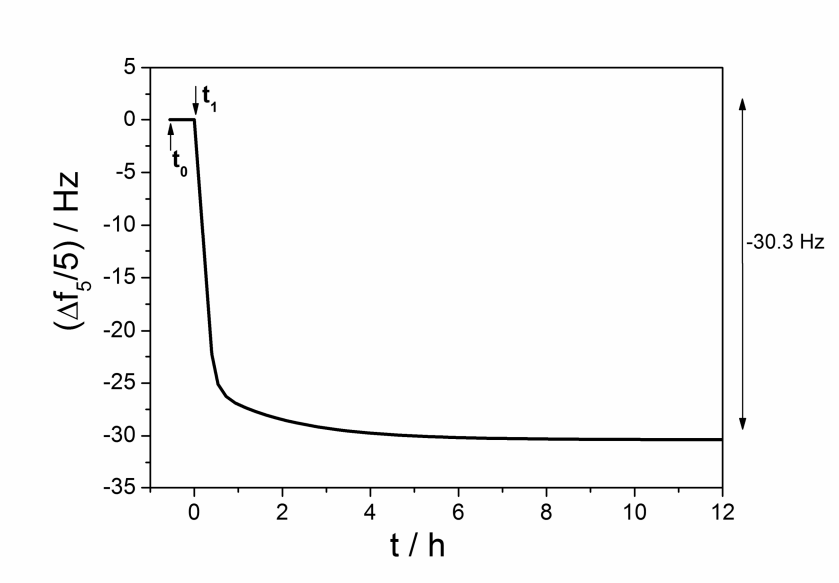


**Figure S1.** Time resolved shift of the normalized 5th overtone frequency ($\Delta f_5/5$) measured for a 5 MHz quartz crystal plate initially facing pure ethanol and upon the injection of a MPA 1 mM solution in pure ethanol. The arrows indicate the times for injection of pure ethanol ($t_0$), and MPA ($t_1$). Temperature was kept at 25º C in all measurements.

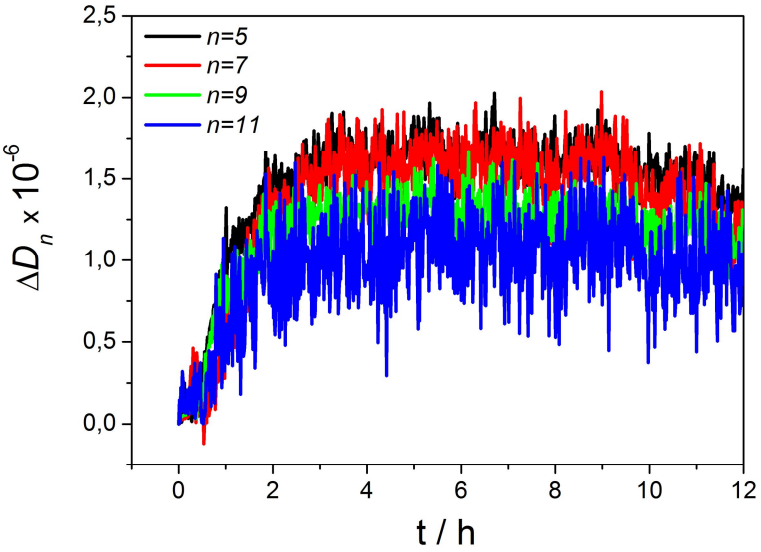


**Figure S2.** Time resolved shift of the dissipation factor ($\Delta D_n$) measured at different overtones ($n$) in simultaneous with the frequency data presented in Fig S1.

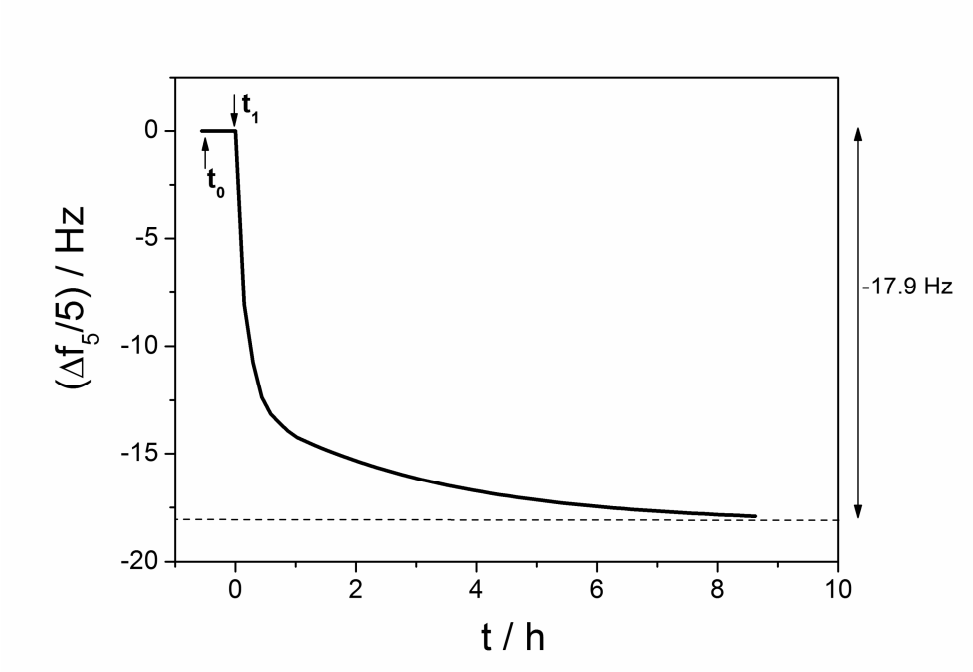


**Figure S3.** Time resolved shift of the normalized 5th overtone frequency ($\Delta f_5/5$) measured for a 5 MHz quartz crystal plate initially facing 0.05 M acetate buffer solution (pH=5.5) and upon the injection of 1 mg mL$^{-1}$ Chit95 solution in the same buffer. The arrows indicate the times for injection of pure ethanol ($t_0$), and Chit95 ($t_1$). Temperature was kept at 25º C in all measurements.

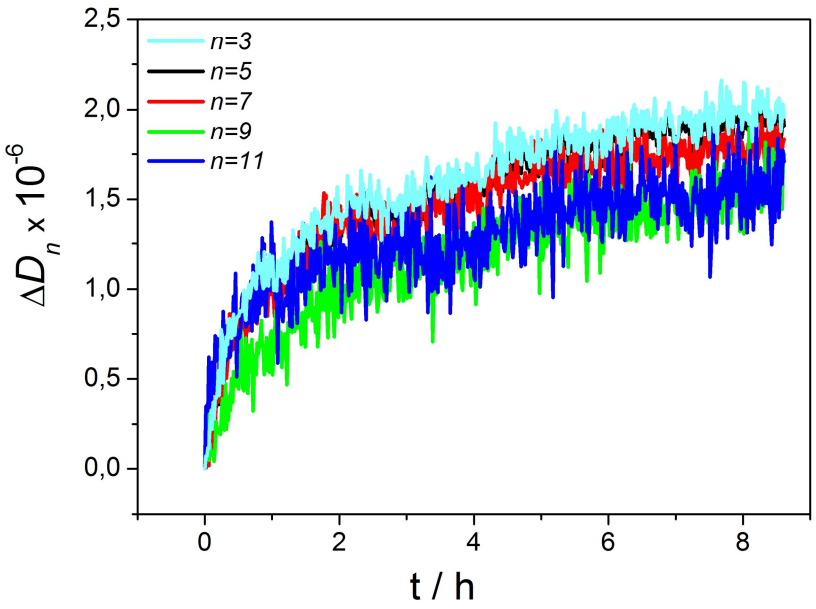


**Figure S4.** Time resolved shift of the dissipation factor ($\Delta D_n$) measured at different overtones ($n$) in simultaneous with the frequency data presented in Fig S3.

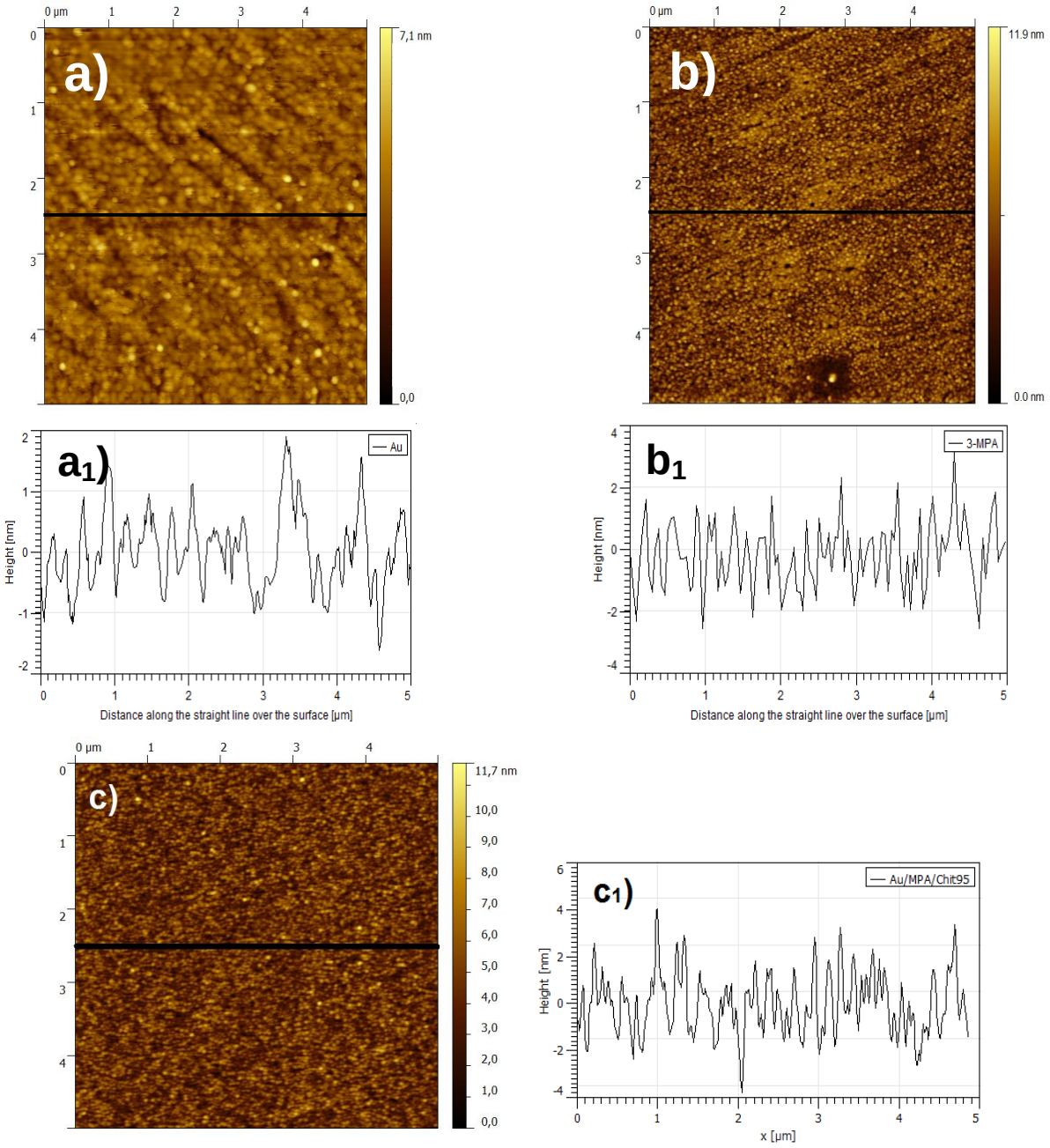


**Figure S5.** AFM topographic images taken in tapping mode over 5 µm × 5 µm regions of bare Au quartz plates **(a)** and the different model substrates used for the adsorption of $F(ab')_2$ in this work: Au/MPA **(b)** and Au/MPA/Chit95 **(c)**. The regions displayed were representative of the full samples. The height profiles along the lines drawn in the images have been also extracted in each case **($a_1$, $b_1$**, and **$c_1$)**.

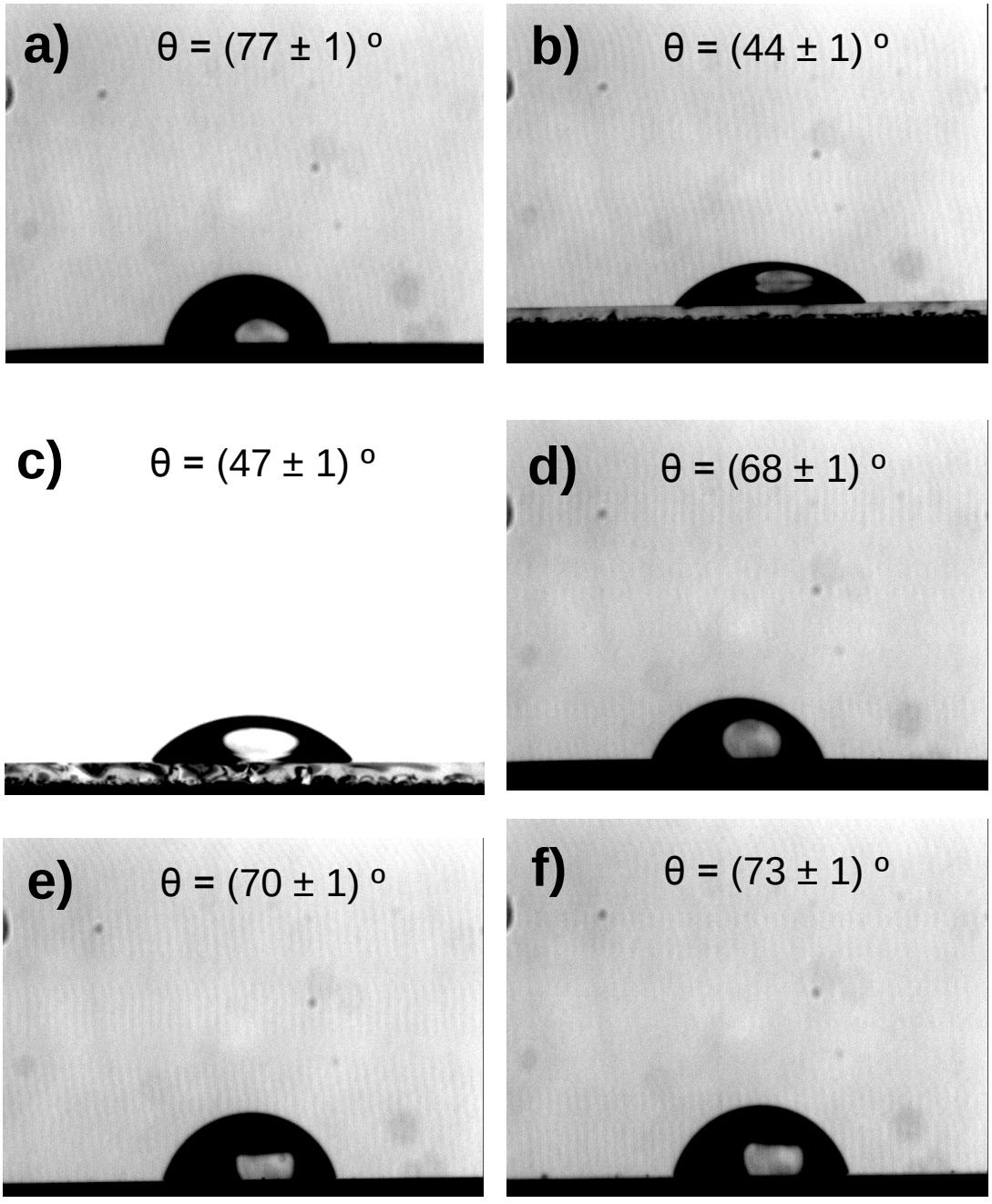

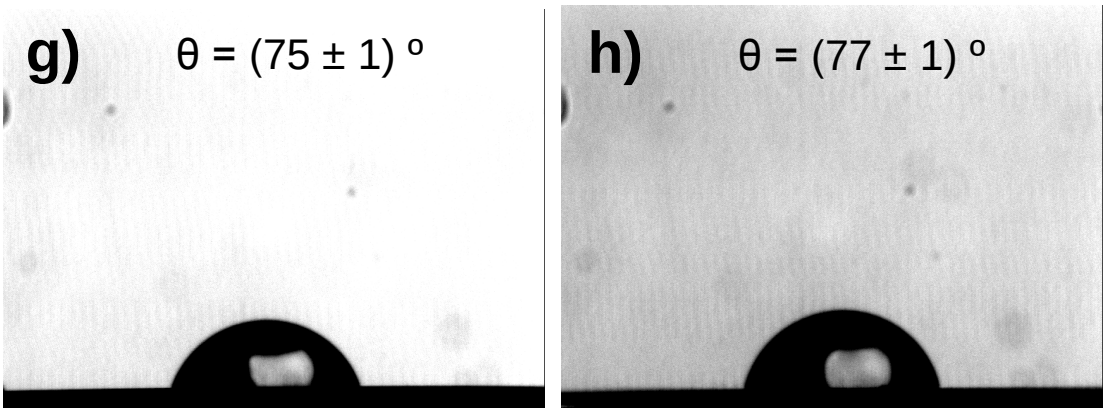


**Figure S6.** Changes in the contact angle measured for Au/MPA/F(ab´)$_2$ surfaces prepared from goat anti-human F(ab´)$_2$ (Fab specific) + 0.01 M PBS solutions (pH 6.85) with the following $C_{Fab2}$: 0.03 (**d**), 3.0 (**e**), 9.1 (**f**), 45.7 (**g**), and 128.6 μg mL$^{-1}$ (**h**). The pictures for sessile drops formed on bare Au (**a**), Au/MPA (**b**), and Au/MPA/Chit95 (**c**), are included for comparison.

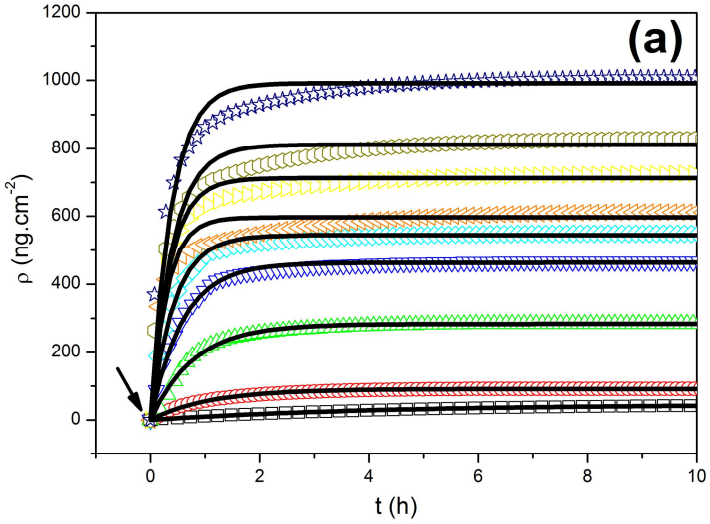


**Figure S7.** Time resolved shift in the surface mass density ($\rho_{Fab2}$) sensed for a 5 MHz quartz crystal plate during 10 h, upon the injection of the following F(ab´)$_2$: 0.03 (black empty squares), 0.3 (red empty circles), 3.0 (green empty up triangles), 9.1 (blue empty down triangles), 15.2 (cyan empty diamonds), 30.5 (orange empty left triangles), 45.7 (yellow empty right triangles), 60.9 (dark yellow empty hexagons), and 128.6 μg·mL$^{-1}$ (navy empty stars), in 0.010 M phosphate buffer (pH = 6.85). The injection of the antibody fragment is indicated by a black arrow. The black straight lines represent kinetic fittings of the experimental data to the single exponential equation based on the Random Sequential Adsorption (RSA) model (eq. 9). The normalized 5$^{th}$ overtone frequency ($\Delta f_5/5$; 25 MHz) was used in all cases to calculate $\rho_{Fab2}$ through the Sauerbrey's model (eq. 3). Temperature was kept at 25º C in all measurements.

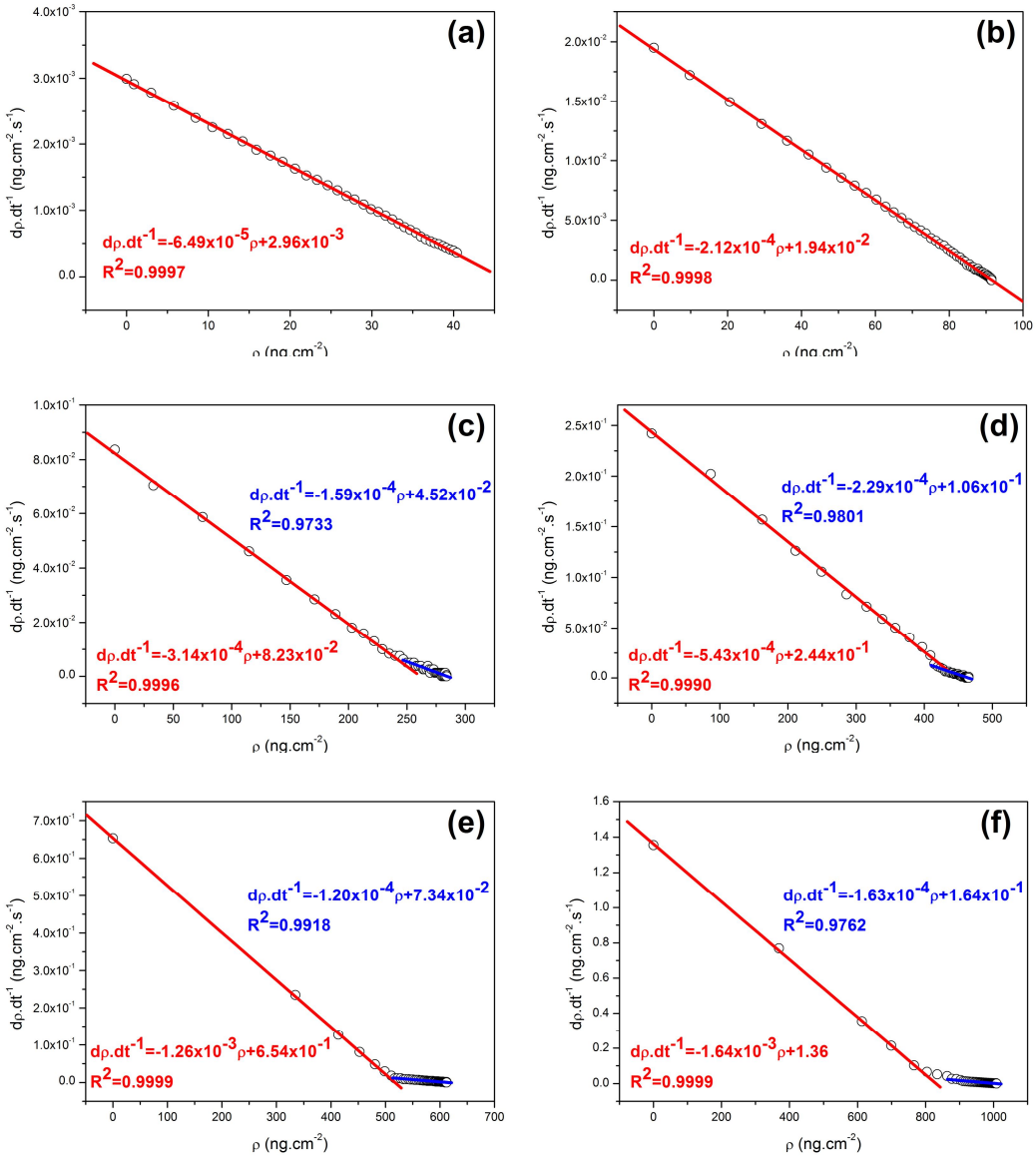


**Figure S8.** $dr_{Fab2}/dt^{-1}$ vs $\rho_{Fab2}$ plots derived for some of the kinetic curves presented in Fig S7: 0.03 **(a)**, 0.3 **(b)**, 3.0 **(c)**, 9.1 **(d)**, 30.5 **(e)**, and 128.6 μg mL$^{-1}$ **(f)** F(ab´)$_2$ solutions in 0.010 M phosphate buffer (pH = 6.85). With the exception of panels **a)** and **b)**, the adsorption rate decreased in all the cases with different slopes after exceeding a certain critical value of $\rho_{Fab2}$, as indicated by the linear regression of the data in the different regions (red and blue straight lines).

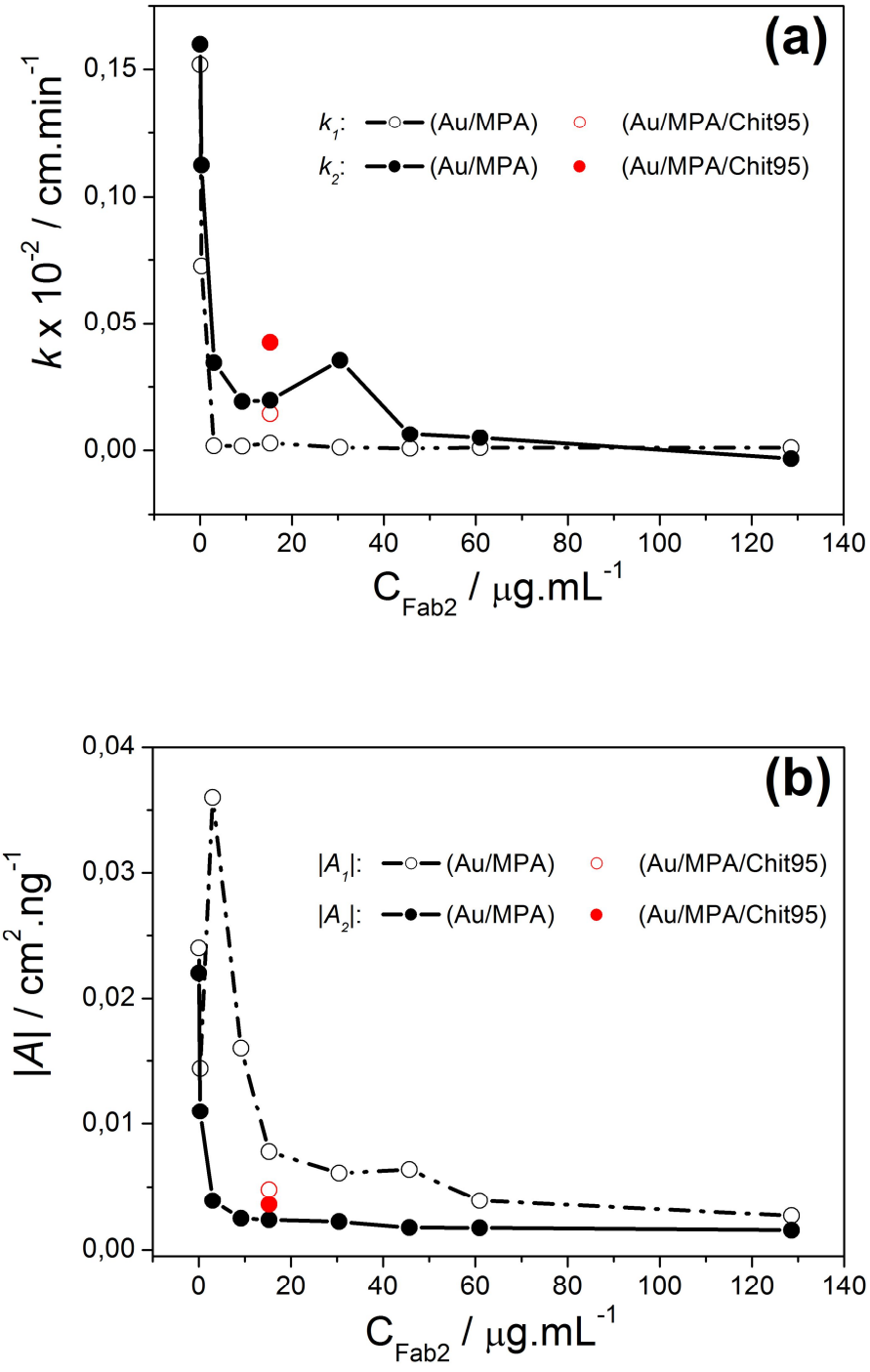


**Figure S9.** Evolution of rate constants **(a)** and steric factors **(b)** associated to surface attachment ($k_1$ and $|A_1|$, empty circles) and rearrangement ($k_2$ and $|A_2|$, full circles) of F(ab´)$_2$ adsorbed onto Au/MPA (black data) and Au/MPA/Chit95 (red) with increasing $C_{Fab2}$. These parameters were obtained by fitting the curves in Fig S7 to Eq. 10

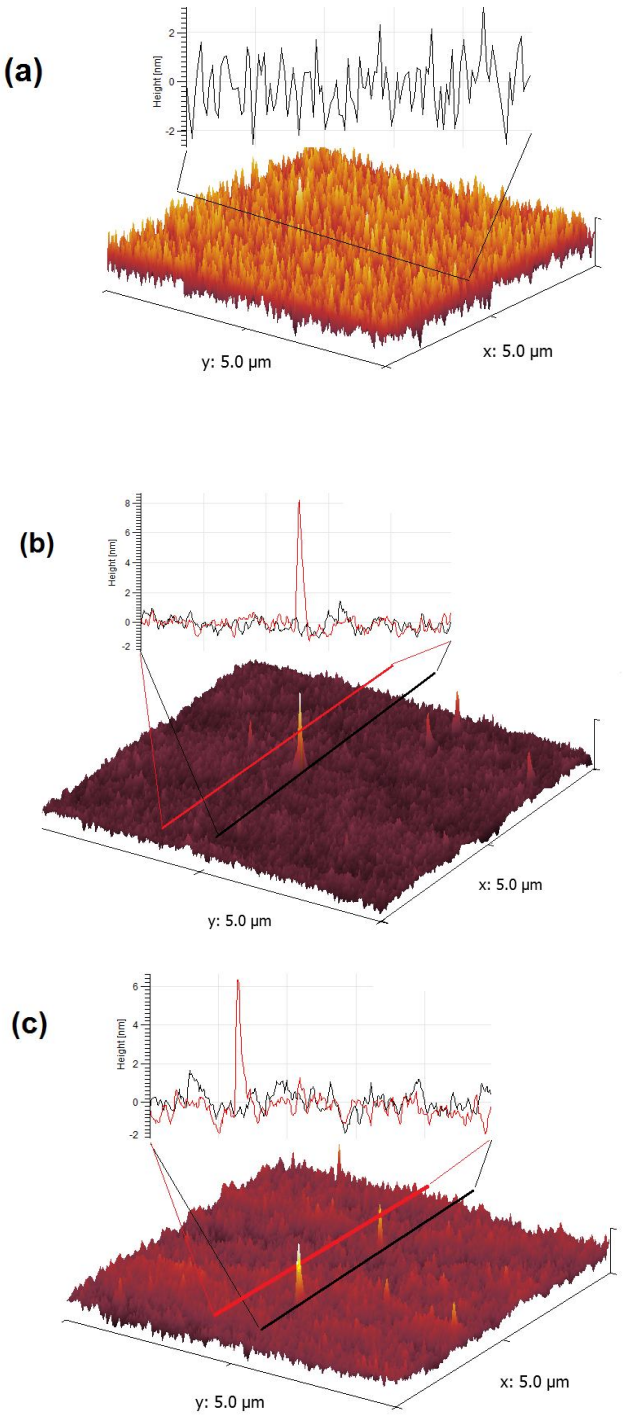


**Figure S10.** AFM topographic images (3D views) taken in tapping mode over 5 µm × 5 µm regions of the quartz plates modified with Au/MPA **(a)** and Au/MPA/F(ab´)$_2$ prepared with 10 h from F(ab´)$_2$ solutions 10 mM PBS (pH 6.85) with $C_{Fab2}$=30.5 (**b**) and 128.6 µg mL$^{-1}$ (**c**). The height profiles along the black and red lines drawn in the images, are presented above the topographies.

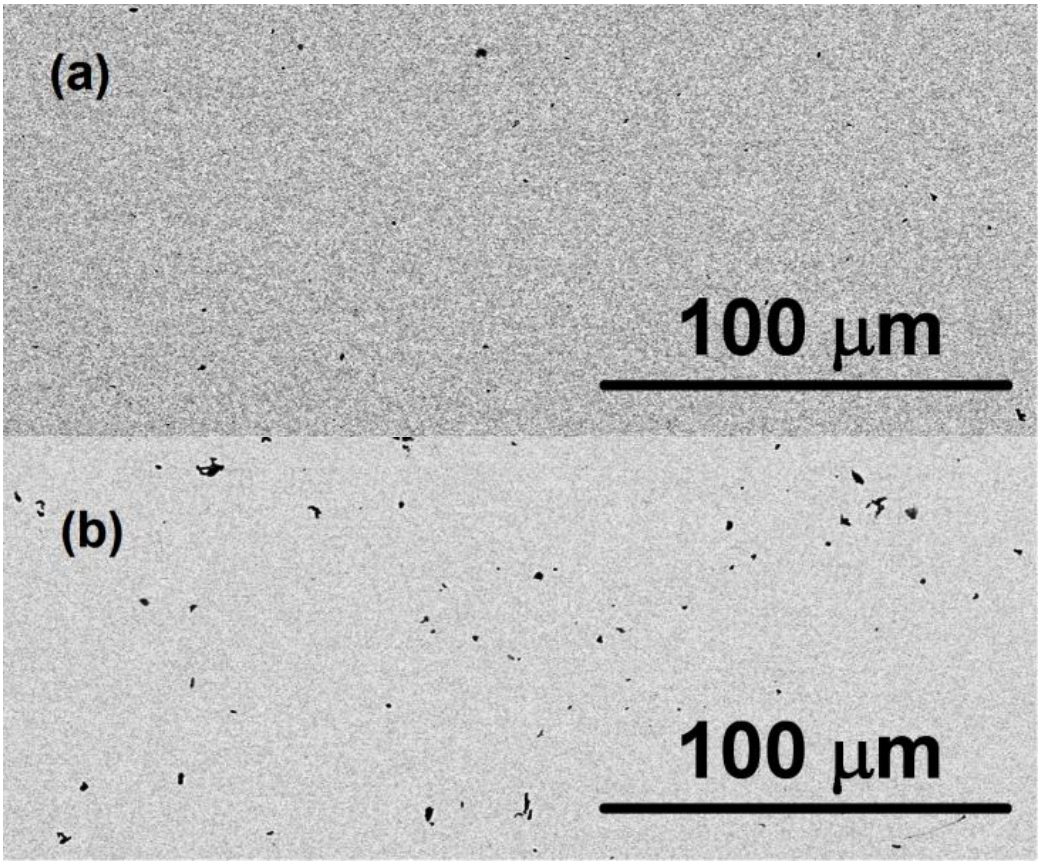


**Figure S11.** SEM pictures obtained in backscattered electrons (BSED) mode for the Au/MPA/F(ab´)$_2$ quartz plates prepared with 10 h from 30.5 **(a)** and 128.6 μg·mL$^{-1}$**(b)** F(ab´)$_2$ solutions in 0.01 M PBS (pH 6.85).

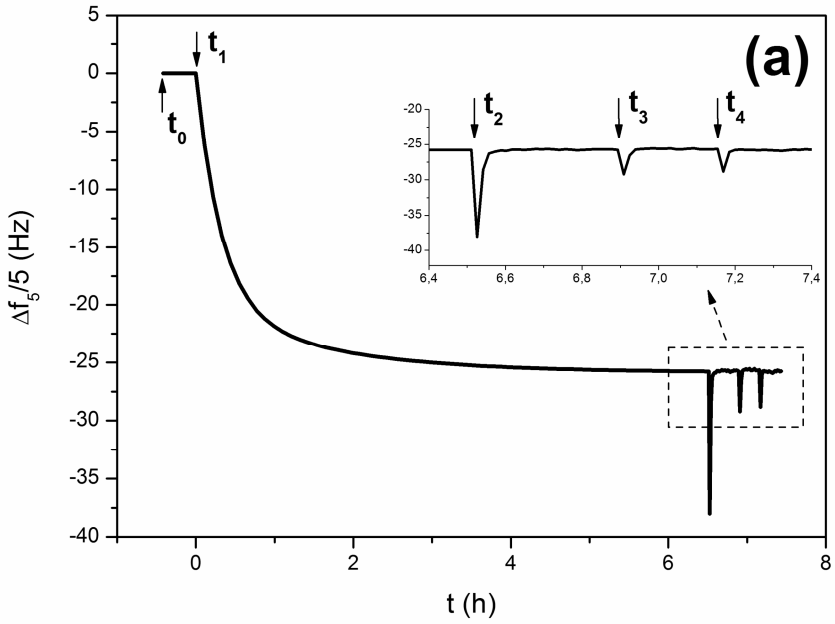
(a)
t0
t1
t2
t3
t4
Δf5/5 (Hz)
t (h)

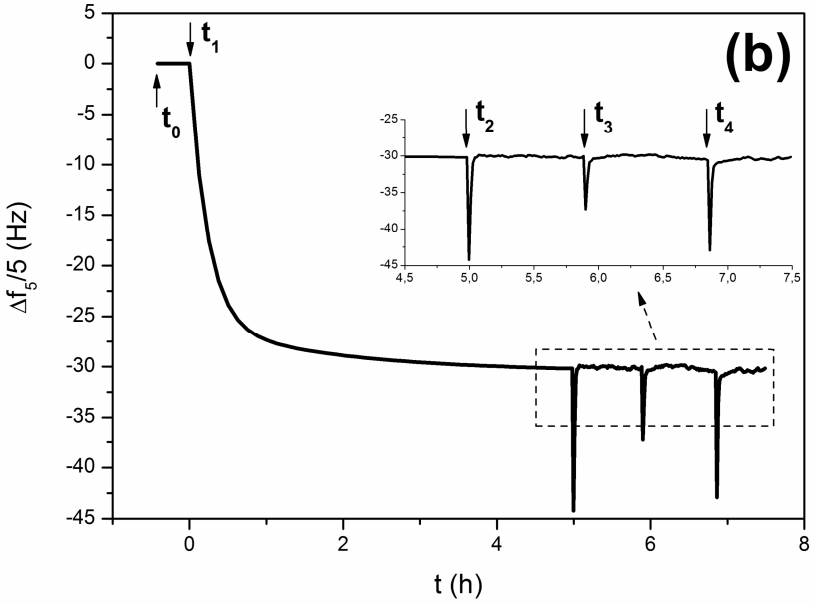
(b)
t0
t1
t2
t3
t4
Δf5/5 (Hz)
t (h)

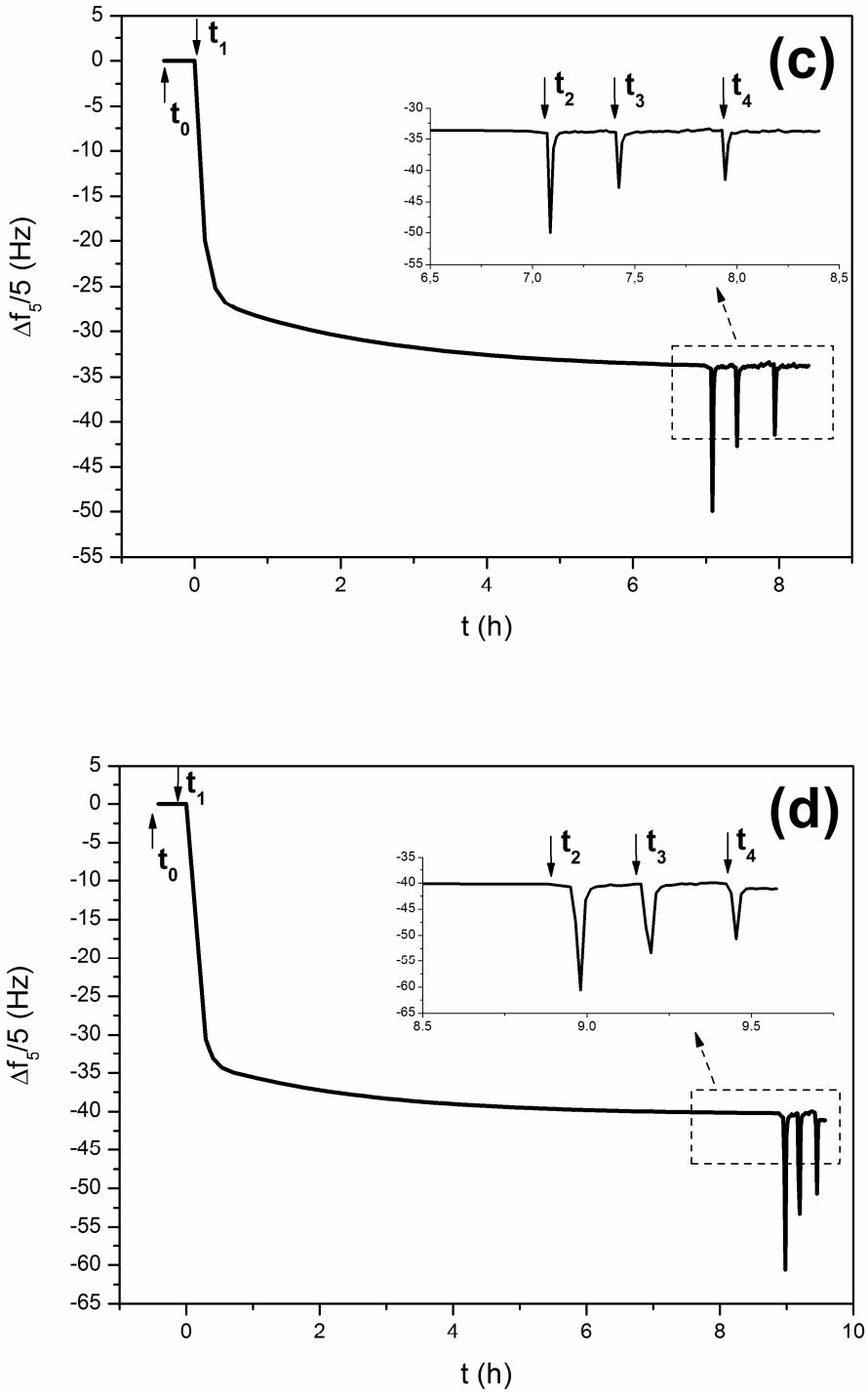


**Figure S12.** Kinetic curves (black lines) obtained during adsorption of F(ab´)$_2$ from 0.01 M PBS (pH 6.85) solutions (injected at $t_1$) with the following $C_{Fab2}$: 9.1 (**a**), 15.2 (**b**), 30.5 (**c**), and 45.7 µg·mL$^{-1}$ (**d**). PBS buffer was repeatedly injected at times longer than 5h as indicated by the arrows at times $t_2$, $t_3$, and $t_4$. The inset shows a detailed view of the changes induced by the buffer rinsing.

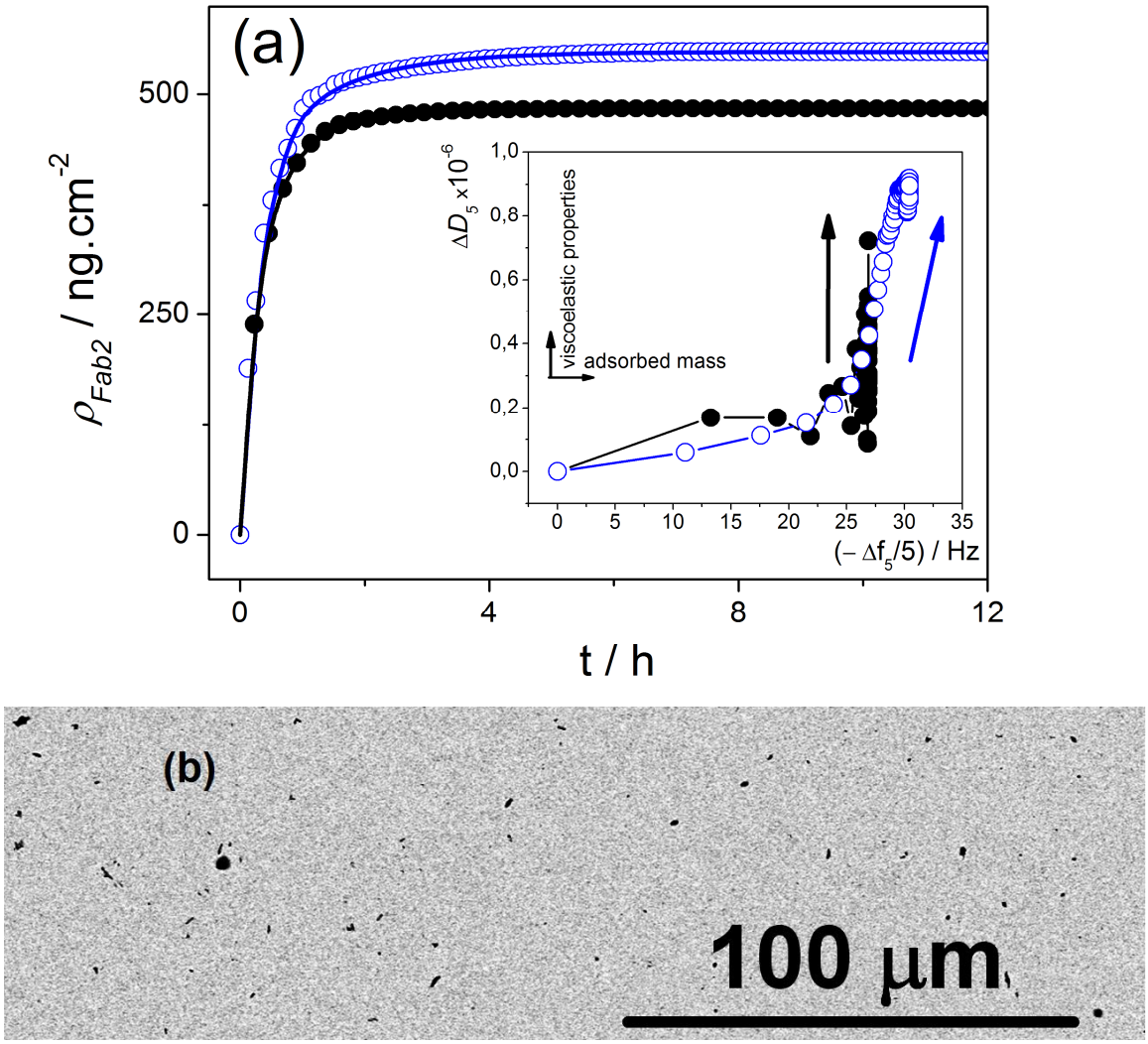


**Figure S13.** (a) Changes in surface mass density registered upon adsorption of F(ab´)$_2$ ($r_{Fab2}$) onto Au/MPA (blue empty circles) and Au/MPA/Chit95 (black filled circles) from a 15.2 mg·mL$^{-1}$ solution in PBS 0.01 M (pH 6.85). $r_{Fab2}$ was calculated from $Df_5/5$ data through the Sauerbrey´s model. The data were fitted to eq 10 in both cases (blue and black straight lines respectively). The inset shows the corresponding $DD_5$ *vs* $Df_5/5$ plots. (b) *Ex-situ* SEM images were obtained for the Au/MPA/Chit95/F(ab´)$_2$ plate at the end of the process.

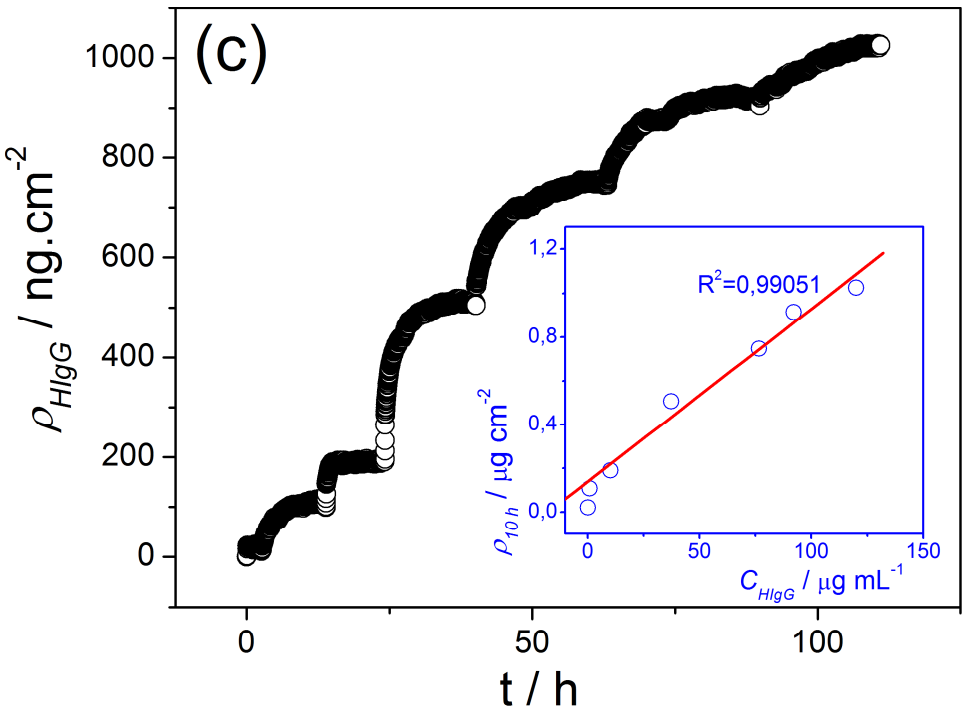


**Figure S14.** Changes registered in $r_{HIgG}$ for Au/MPA/Chit95/F(ab´)$_2$ plates after the consecutive injection of aliquots of HIgG stock solution (0.06, 0.86, 10.15, 37.34, 76.53, 92.1, and 130 mg·mL$^{-1}$) into the QCM-D cell. After each addition, measurements were taken for at least 10 h. Plateau uptakes ($r_{10h}$) are plotted vs. $C_{HIgG}$ (blue empty circles) and fitted to a straight line (red line) in the inset.

**Table S1.** Surface roughness ($R_{MS}$), average height ($H_{AV}$), and apparent particle size obtained from the 5 μm × 5 μm AFM topographic images in Fig S5 after polynomial levelling using the freeware Gwyddion 2.25.

| Surface | $R_{MS}$ / nm | $H_{AV}$ / nm | d / nm |
|---|---|---|---|
| **Bare Au** | 2.08 | 3.82 | 60-100 |
| **Au/MPA** | 1.25 | 4.02 | 40-60 |
| **Au/MPA/Chit95** | 1.28 | 4.57 | 40-60 |

## References

[1] Stoscheck, C. M. *Meth. Enzymol.* **1990**, *182*, 50.

[2] Campiña, J. M.; Souza, H. K. S.; Borges, J.; Martins, A.; Gonçalves, M. P.; Silva, F. *Electrochim. Acta*, **2010**, *55*, 8779.

[3] Campiña, J. M.; Martins, A.; Silva, F. *Electrochim. Acta* **2008**, *53*, 7681.

[4] Trasatti, S.; Pettri, O.A. *J. Electroanal. Chem.* **1992**, *327*, 353.

[5] Jarzabek, G.; Borowska, Z. *Electrochim. Acta* **1997**, *19*, 2915.

[6] Dickertmann, D.; Koppitz, F.D.; Schultze, J.W. *Electrochim. Acta* **1976**, *21*, 967.

[7] Sauerbrey, G.; *Zeitschrift für Physik*, **1959**, *155*, 206.

[8] Murray, B. S.; Cros, L. *Colloid Surface B* **1998**, *10*, 227; Murray B. S.; Deshaires, C. *J. Colloid Interface Sci.* **2000**, *227*, 32.

[9] Baba, A.; Kaneko, F.; Advíncula, R. C. *Colloids Surface A* **2000**, *173*, 39.

[10] Ferreyra, N. F.; Coché-Guerénte, L.; Labbé, P.; Calvo, E.; Solís, V. M. *Langmuir*, **2003**, *19*, 3864.

[11] Rényi, A. *Publ. Math. Inst. Hung. Acad. Sci.* **1958**, *3*, 109.

[12] Schaaf, P.; Talbot, J. *J. Chem. Phys.* **1989**, *91*, 4401.

[13] Ramsden, J. J. *Phys. Rev. Lett.* **1993**, *71*, 295.

[14] Anand, G.; Sharma, S.; Dutta, A. K.; Kumar, S. K.; Belfort, G. *Langmuir* **2010**, *26*, 10803.

[15] Jamadagni, S. N.; Godawat, R.; Dordick J. S.; Garde, S. *J. Phys. Chem. B* **2009**, *113*, 4093.

[16] Rabe, M.; Verdes D., Seeger, S. *Adv. Colloid Interface Sci.* **2011**, *162*, 87.

[17] Sethuraman, A.; Belfort, G. *Biophys. J.* **2005**, *88*, 1322.

[18] Schaaf, P.; Talbot, J. *J. Chem. Phys.* **1989**, *91*, 4401.

[19] Minton, A. P. *Biophys. Chem.* **2000**, *86*, 239.

[20] Minton, A. P. *Biophys. J.* **2001**, *80*, 1641.